Fluorescence correlation spectroscopy analysis of segmental dynamics in actin filaments

Anne Bernheim-Groswasser, Roman Shusterman, and Oleg Krichevsky

Citation: The Journal of Chemical Physics **125**, 084903 (2006); doi: 10.1063/1.2244550
View online: https://doi.org/10.1063/1.2244550
View Table of Contents: http://aip.scitation.org/toc/jcp/125/8
Published by the American Institute of Physics

Fluorescence correlation spectroscopy analysis of segmental dynamics in actin filaments

Anne Bernheim-Groswasser
Chemical Engineering Department, Ben-Gurion University, Beer-Sheva 84105, Israel;
Reimund Stadler Minerva Center, Ben-Gurion University, Beer-Sheva 84105, Israel;
and Ilse Kats Center for Nanoscience, Ben-Gurion University, Beer-Sheva 84105, Israel

Roman Shusterman
Physics Department, Ben-Gurion University, Beer-Sheva 84105, Israel

Oleg Krichevsky[a)]
Physics Department, Ben-Gurion University, Beer-Sheva 84105, Israel
and Ilse Kats Center for Nanoscience, Ben-Gurion University, Beer-Sheva 84105, Israel

(Received 27 March 2006; accepted 6 July 2006; published online 22 August 2006)

We adapt fluorescence correlation spectroscopy (FCS) formalism to the studies of the dynamics of semiflexible polymers and derive expressions relating FCS correlation function to the longitudinal and transverse mean-square displacements of polymer segments. The obtained relations do not depend on any specific model of polymer dynamics. We use the derived expressions to measure the dynamics of actin filaments in two experimental situations: filaments labeled at distinct positions and homogeneously labeled filaments. Both approaches give consistent results and allow to measure the temporal dependence of the segmental mean-square displacement over almost five decades in time, from ~ 40 μs to ~ 2 s. These noninvasive measurements allow for a detailed quantitative comparison of the experimental data to the current theories of semiflexible polymer dynamics. Good quantitative agreement is found between the experimental results and theories explicitly accounting for the hydrodynamic interactions between polymer segments. © *2006 American Institute of Physics*. [DOI: 10.1063/1.2244550]

I. INTRODUCTION

Living cells have remarkable mechanical properties which enable them to move, divide, and respond to external stresses. These properties are mainly attributed to the dynamical characteristics of the cell cytoskeleton, which is a complex three-dimensional network of protein filaments mostly comprised of F-actin and microtubules. Both types of filaments are the polymerized forms of monomeric protein subunits: globular actin (G-actin) and tubulin, respectively. The cytoskeleton derives its strength from the elastic properties of these biopolymers, which, unlike synthetic polymers, are characterized by a high bending rigidity.

The polymer rigidity is described by a persistence length l_p above which thermal fluctuations can efficiently bend the polymer. Semiflexible polymers such as F-actin and microtubules have a long persistence length: $l_p \sim 17$ μm for F-actin[1] and several millimeters for microtubules, orders of magnitude larger than those of synthetic polymers. The large rigidity of these biological polymers enables us to experimentally address the fundamental questions of polymer dynamics at the subpersistence length scales. The dynamics and the mechanical properties of F-actin and microtubule networks were studied by different optical techniques, such as dynamic light scattering,[2] fluorescence imaging,[3,4] diffusive wave spectroscopy (DWS), and microrheology.[5–9]

One of the most detailed features of polymer dynamics accessible in experiments is the kinetics of monomer motion measured by the temporal dependence of monomer's mean-square displacement (MSD) $\langle \Delta r^2(t) \rangle$. For length scales below the persistence length, the monomer displacements are anisotropic with a major contribution coming from the transverse modes (displacements perpendicular to the polymer contour) and only a minor contribution from longitudinal modes. Theories[10–17] predict that the kinetics of transverse motion, and thus the overall monomer's MSD, should follow the power law dependence of $\langle \Delta r^2 \rangle \propto t^{3/4}$.

A feature related to the monomer MSD, the time dependence of the longitudinal fluctuations was obtained by measuring the end-to-end distance of individual actin filaments visualized by fluorescence video microscopy.[4] Although the data are consistent with theoretically predicted dependence, the temporal resolution of video microscopy limits the measurements to time scales larger than 80 ms and thus the overall range of $\propto t^{3/4}$ dependence spans over one order of magnitude in time only.[4]

A wide range of time scales was assessed using DWS and microrheology of micron-sized beads inserted into the F-actin mesh.[5,8] The $\langle \Delta r^2 \rangle \propto t^{3/4}$ scaling was observed from ~ 10 μs to ~ 10 ms. However, it is not quite clear how the MSD of a bead is related to the actual monomers' displacements. While the beads' motion depends on the properties of the mesh, the beads themselves may affect the dynamics of the filaments, e.g., via their large friction coefficient.[5] In par-

[a)]Electronic mail: okrichev@bgu.ac.il

ticular, the monomer kinetics measured by fluorescence video microscopy[4] is two orders of magnitude faster than the motion of the beads measured by DWS.[5]

Here we present a new noninvasive approach to measure the monomers' MSD in stiff filaments: the filaments are tagged with fluorescent labels and the segmental dynamics of the filaments is then followed with fluorescence correlation spectroscopy (FCS) technique. We show that FCS correlation function is directly related to the temporal dependence of monomers' MSD $\langle \Delta r^2(t) \rangle$. The measurement of the FCS correlation function allows us to obtain the kinetics of F-actin monomer motion over a wide range of time scales, from 40 μs to 2 s. Previously, the same method was used to study monomer dynamics in DNA polymers[18,19] and also very recently to study the internal dynamics of F-actin.[20] While in terms of the experimental technique our method is similar to that of Winkler *et al.*,[20] our approach to analysis of FCS measurements differs from theirs significantly. Winkler *et al.* base their analysis on a specific model of semiflexible polymer dynamics[12] which, in particular, assumes isotropic monomer motion. They derive the predictions of this model for FCS correlation functions and fit them to the measured correlation functions directly.

In contrast to the approach of Winkler *et al.* we derive a formalism relating monomer MSD to FCS correlation functions in a model-independent manner, and then compare measured $\langle \Delta r^2(t) \rangle$ with the predictions of different polymer dynamic theories. While the standard formulas of FCS can be applied to double-stranded DNA, new expressions relating FCS correlation function to monomer MSD have to be derived for stiff filaments such as F-actin and used to analyze experimental data. The main reason for that is the large difference in the persistence lengths of DNA and F-actin. In general, the dynamics of a semiflexible polymer is anisotropic: the segmental motions transverse to the filament are larger than longitudinal displacements. This anisotropy is lost at the length scales above polymer persistence length. For DNA, $l_p \approx 50$ nm is much smaller than typical dimensions of FCS sampling volume ($\sim$500 nm) and the expressions implying isotropic dynamics can be used in all of the dynamic range probed by FCS. For actin filaments with $l_p \approx 17$ μm the situation is reversed and the anisotropy of segmental motion has to be taken into account explicitly.

In the next section we derive the FCS expressions for anisotropic motion of stiff filaments. Although the segmental motion is dominated by the transverse component, for the sake of generality, we will derive expressions which take into account explicitly both transverse and longitudinal displacements. Then we use these expressions to analyze the results of two sets of experiments with different labeling strategies: (1) partially (or locally) labeled filaments (obtained via polymerization of nonfluorescent monomeric actin on fluorescent seeds) and (2) homogeneously labeled filaments (obtained by polymerization of F-actin from a mixture of labeled and unlabeled actin monomers). We note that the second labeling strategy is similar to that used by Winkler *et al.*[20] The analysis of the experimental data with the expressions appropriate to each of these cases gives consistent results on temporal dependence of monomer's MSD. Finally, the experimental data are compared to theoretical predictions for the dynamics of semiflexible chains. The results are in qualitative and *quantitative* agreement with the theories taking into account hydrodynamic interactions between the polymer segments.[14,15]

II. THEORY

FCS technique[21–23] (reviewed in, e.g., Refs. 24–27) is based on monitoring fluctuations $\delta I_{\mathrm{em}}(t) = I_{\mathrm{em}} - \langle I_{\mathrm{em}} \rangle$ in fluorescence emission $I_{\mathrm{em}}(t)$ as fluorescence species diffuse in a spatially restricted excitation field, formed typically with the help of confocal optical scheme.[28] The autocorrelation function $G(t) = \langle \delta I_{\mathrm{em}}(0) \delta I_{\mathrm{em}}(t) \rangle$ of emission fluctuations reflects the kinetics of motion of fluorescent sources.

In this section we adapt the general formalism of FCS to the case of dynamics of linear stiff polymers and derive expressions relating FCS correlation function to the temporal dependence of MSD $\langle \Delta r^2(t) \rangle$ of polymer segments.

The instantaneous detected emission, average emission, and the correlation function of fluorescence fluctuations are found through the spatial distribution $c(\mathbf{r},t)$ of fluorescent labels and excitation-detection profile $I(\mathbf{r})$,[22]

$$I_{\mathrm{em}}(t) = Q \int d\mathbf{r} I(\mathbf{r}) c(\mathbf{r},t),$$

$$\langle I_{\mathrm{em}} \rangle = Q \bar{c} \int d\mathbf{r} I(\mathbf{r}), \tag{1}$$

$$G(t) = Q^2 \int d\mathbf{r} d\mathbf{r}' I(\mathbf{r}) I(\mathbf{r}') \langle \delta c(\mathbf{r},0) \delta c(\mathbf{r}',t) \rangle, \tag{2}$$

where Q is specific brightness of a fluorescent molecule dependent on fluorophore properties and the efficiency of detection optics, $\bar{c} = \langle c(\mathbf{r},t) \rangle$ is the average concentration of fluorophores, and $\delta c(\mathbf{r},t) = c(\mathbf{r},t) - \bar{c}$. Following Ref. 29 Eq. (2) can be rewritten as

$$G(t) = \frac{(2\pi)^3 Q^2}{V} \int d\mathbf{q} |\tilde{I}(\mathbf{q})|^2 \langle \delta \tilde{c}^*(\mathbf{q},0) \delta \tilde{c}(\mathbf{q},t) \rangle, \tag{3}$$

where "tilde" denotes spatial Fourier transform of the corresponding quantities, such as, e.g., $\tilde{I}(\mathbf{q}) = (2\pi)^{-3/2} \int d\mathbf{r} I(\mathbf{r}) e^{-i\mathbf{q}\mathbf{r}}$, and V is the total volume of the sample.

We assume that fluorescent molecules are not moving independently but are attached to relatively large objects which themselves move independently of each other. We will further assume that the objects are statistically equivalent and that the distribution of fluorophores within each object with respect to its center of mass is described by $\Phi(\mathbf{r}, \hat{s}(t))$, where $\hat{s}(t)$ denotes the set of internal degrees of freedom describing the current conformation and the orientation of the object. Then $c(\mathbf{r},t) = \Sigma_j \Phi(\mathbf{r} - \mathbf{r}_j(t), \hat{s}_j(t))$, $\tilde{c}(\mathbf{q},t) = \Sigma_j \tilde{\Phi}(\mathbf{q}, \hat{s}_j(t)) e^{-i\mathbf{q}\mathbf{r}_j(t)}$, where $\mathbf{r}_j(t)$ and $\hat{s}_j(t)$ define, respectively, the center-of-mass position and internal conformation of object j at time t. Finally, substituting these formulas in Eq. (3) we have

$$G(t) = (2\pi)^3 Q^2 \bar{n} \int d\mathbf{q} |\tilde{I}(\mathbf{q})|^2 \langle \tilde{\Phi}^*(\mathbf{q}, \hat{s}(0)) \times \tilde{\Phi}(\mathbf{q}, \hat{s}(t)) e^{-i\mathbf{q}\Delta\mathbf{r}(t)} \rangle, \quad (4)$$

where $\bar{n}$ is the average concentration of the objects (number of objects per unit volume), $\Delta\mathbf{r}(t) = \mathbf{r}_j(t) - \mathbf{r}_j(0)$ is the displacement of an object, and the index j was omitted everywhere in Eq. (4) due to the statistical equivalence of the objects.

In its general form Eq. (4) can be applied to any objects which have some internal structure and internal dynamics.

We assume now that the objects are uniformly labeled segments of semiflexible polymers (one labeled segment of length L per polymer; total polymer length l, in general, is larger than L, i.e., polymers may contain unlabeled parts). For sufficiently stiff polymers, we can neglect the dynamics within the labeled segments and consider them to be straight. In this case the set of internal degrees of freedom $\hat{s}$ reduces to a unit vector $\mathbf{s}$ defining the orientation of the segment. Within the same approximation we can assume that any given labeled segment moves without change in its orientation $\mathbf{s}_j(0) = \mathbf{s}_j(t)$. We will discuss in detail the validity of our assumptions at the end of this section. Here we just note that although these assumptions may look prohibitively restrictive, for sufficiently stiff filaments they are valid in a wide range of segmental displacements.

For a thin straight segment of length L uniformly labeled with linear density σ of fluorophores,

$$\tilde{\Phi}(\mathbf{q}, \mathbf{s}) = \frac{\sigma}{\pi\sqrt{2\pi}} \frac{\sin((1/2)\mathbf{q}\mathbf{s}L)}{\mathbf{q}\mathbf{s}} = \frac{\sigma}{\pi\sqrt{2\pi}} \frac{\sin((1/2)qL\cos\alpha)}{q\cos\alpha}, \quad (5)$$

where α is an angle between $\mathbf{q}$ and $\mathbf{s}$. Furthermore, we split the segmental displacement into components parallel and perpendicular to the segment $\Delta\mathbf{r} = \Delta\mathbf{r}_\parallel + \Delta\mathbf{r}_\perp$, we assume the two components to be independent of each other and to be Gaussian random variables. Then, for fixed $\mathbf{q}$ and $\mathbf{s}$ the ensemble average of $e^{-i\mathbf{q}\Delta\mathbf{r}(t)}$ is given by

$$\langle e^{-i\mathbf{q}\Delta\mathbf{r}(t)} \rangle_{|\mathbf{q},\mathbf{s}} = \exp\left(-\frac{q^2\cos^2\alpha}{2} \langle \Delta r_\parallel^2 \rangle - \frac{q^2\sin^2\alpha}{4} \langle \Delta r_\perp^2 \rangle \right). \quad (6)$$

The difference in the numeric prefactors in the two terms in the Eq. (6) stems from the fact that $\Delta\mathbf{r}_\parallel$ is defined on a line (parallel to $\mathbf{s}$), while $\Delta\mathbf{r}_\perp$ is defined in a plane (perpendicular to $\mathbf{s}$).

We assume, as it is usually done for confocal setups, the excitation-detection profile $I(\mathbf{r})$ to be three-dimensional (3D) Gaussian axisymmetric with respect to optical axis Z,

$$I(\mathbf{r}) = I_0 \exp\left(-\frac{2(x^2+y^2)}{w_{xy}^2} - \frac{2z^2}{w_z^2} \right), \quad (7)$$

$$\tilde{I}(\mathbf{q}) = \frac{I_0 w_{xy}^2 w_z}{8} \exp\left(-\frac{w_{xy}^2}{8} q^2 \sin^2\theta - \frac{w_z^2}{8} q^2 \cos^2\theta \right), \quad (8)$$

where w_{xy} and w_z define the width of the profile in the XY plane and in Z direction, respectively, and θ is an angle between $\mathbf{q}$ and Z axis.

Substituting (5), (6), and (8) into Eq. (4), averaging over α for a given $\mathbf{q}$ and integrating over $\mathbf{q}$, we have

$$G(t) = \frac{\pi}{16} I_0^2 w_{xy}^5 \omega^2 Q^2 \sigma^2 \bar{n} \int_0^\infty dk \int_{-1}^1 du \int_{-1}^1 \frac{dp}{p^2} \times \sin^2\left(\frac{\lambda k p}{2} \right) \exp\left(-\frac{k^2}{4} f(h_\perp^2, h_\parallel^2, p, u) \right), \quad (9)$$

where $u = \cos\theta$, $p = \cos\alpha$, reduced units $k = q w_{xy}$, $\lambda = L/w_{xy}$, $h_\perp^2 = \langle \Delta r_\perp^2 \rangle / w_{xy}^2$, $h_\parallel^2 = \langle \Delta r_\parallel^2 \rangle / w_{xy}^2$, and $\omega = w_z/w_{xy}$ were introduced, and f denotes the following expression:

$$f(h_\perp^2, h_\parallel^2, p, u) = h_\perp^2 - p^2(h_\perp^2 - 2h_\parallel^2) + u^2(\omega^2 - 1) + 1. \quad (10)$$

FCS correlation function is usually normalized by the square of the average emission $G_1(t) = \langle \delta I_{\mathrm{em}}(0) \delta I_{\mathrm{em}}(t) \rangle / \langle I_{\mathrm{em}} \rangle^2$. With this normalization the amplitude of the correlation function at short time scales is the inverse of the average number N of molecules in the detection volume (given by $\pi^{3/2} w_{xy}^2 w_z$): $G_1(t \to 0) = 1/N$. Here we prefer another normalization: $G_2(t) = \langle \delta I_{\mathrm{em}}(0) \delta I_{\mathrm{em}}(t) \rangle / \langle I_{\mathrm{em}} \rangle = \langle I_{\mathrm{em}} \rangle G_1(t)$. A correlation function defined in this way is independent of the concentration of the moving species (as long as there are no interactions between the objects) and its amplitude at short time scales gives the fluorescence per moving object: $G_2(t \to 0) = \langle I_{\mathrm{em}} \rangle / N$. This is an interesting quantity in the context of labeled segments comparable or larger than w_{xy}: in this case only part of the labeled segment can "fit" into the detection volume and contribute to the correlation function. The length of this part can be estimated from $G_2(t \to 0)$.

In order to calculate $G_2(t)$ we substitute $\bar{c} = \bar{n}\sigma L$ and (7) into (1) to find

$$\langle I_{\mathrm{em}} \rangle = (\pi/2)^{3/2} I_0 w_{xy}^2 w_z Q \bar{n} \sigma L. \quad (11)$$

Performing integration over k in (9) and making use of (11) and of definition of G_2 we obtain

$$G_2(t) = \frac{I_0 Q}{2\sqrt{2}} \sigma w_{xy} \frac{\omega}{\lambda} \int_0^1 du \int_0^1 dp \times \frac{1 - \exp(-\lambda^2 p^2 / f(h_\perp^2, h_\parallel^2, p, u))}{p^2 \sqrt{f(h_\perp^2, h_\parallel^2, p, u)}}. \quad (12)$$

Given the knowledge of the experimental geometry (i.e., parameters w_{xy}, w_z, and L), Eq. (12) can be used to numerically calculate the relation between the FCS correlation function and temporal behavior of segmental MSDs, i.e., $h_\perp^2(t)$ and $h_\parallel^2(t)$.

In two important limiting cases the explicit expressions can be derived for $G_2(t)$: (1) for very short labeled segments, i.e., taking the limit $L \to 0$ while keeping the total amount of labels $P = L\sigma$ finite, and (2) for very long labeled segments, i.e., $L \to \infty$ while $\sigma = \mathrm{const}$.

In the case of short segments, we obtain

$$G_2(t) = \frac{I_0 Q}{2\sqrt{2}} \frac{P\omega}{\sqrt{(1+h_\perp^2)(\omega^2-1)(h_\perp^2-2h_\parallel^2)}} \times \ln \frac{\sqrt{(1+h_\perp^2)(\omega^2+2h_\parallel^2)}+\sqrt{(\omega^2-1)(h_\perp^2-2h_\parallel^2)}}{\sqrt{(1+2h_\parallel^2)(\omega^2+h_\perp^2)}}. \quad (13)$$

We note that for isotropic motion, i.e., for $h_\perp^2=2h_\parallel^2=\langle \Delta r^2\rangle/(3w_{xy}^2)$, Eq. (13) reduces to the more standard FCS expression for the random motion of pointlike objects,

$$G_2(t) = \frac{QI_0}{2\sqrt{2}} P\left(1+\frac{2}{3}\frac{\langle r^2(t)\rangle}{w_{xy}^2}\right)^{-1}\left(1+\frac{2}{3}\frac{\langle r^2(t)\rangle}{w_z^2}\right)^{-1/2}. \quad (14)$$

For infinitely long segments Eq. (12) gives

$$G_2(t) = \frac{QI_0}{2\sqrt{2}} \frac{\sigma w_{xy}\omega\sqrt{\pi}}{\sqrt{(\omega^2-1)(1+h_\perp^2)}} \arctan\sqrt{\frac{\omega^2-1}{1+h_\perp^2}}. \quad (15)$$

Note that $G_2(t)$ in this case is independent of $h_\parallel^2$ since longitudinal motion of infinitely long labeled segments does not lead to any fluctuations in fluorescence.

Although unrelated to our experiments, still an interesting particular case of application of Eq. (15) is that of spherically symmetric detection volume $w_{xy}=w_z=w$. In this case $G_2(t)=\sqrt{\pi/8}QI_0w\sigma(1+h_\perp^2)^{-1}$ is similar to the correlation function produced by a planar motion of pointlike objects.

We return now to Eq. (12) in order to find the dependence of the fluorescence per moving object $G_2(t\to 0)$ on the length of the labeled segment. We make use of the fact that for small segments $L\ll w_{xy}$: $G_2(t\to 0)=QI_0\sigma L/(2\sqrt{2})$ and define an apparent length L_{app} and, respectively, $\lambda_{\mathrm{app}}=L_{\mathrm{app}}/w_{xy}$ such that for the labeled segment of any length $G_2(t\to 0)=QI_0\sigma L_{\mathrm{app}}/(2\sqrt{2})$.

For $t=0$, i.e., $h_\parallel^2=h_\perp^2=0$ it is possible to perform integration over u in Eq. (12) and arrive to the expression relating the apparent length of the labeled segment to its actual length and to the parameters of the detection volume,

$$\lambda_{\mathrm{app}} = \frac{\omega}{\lambda\sqrt{\omega^2-1}}\left[-\ln(\omega+\sqrt{\omega^2-1}) + \int_1^\omega \frac{d\upsilon}{\upsilon\sqrt{\upsilon^2-1}}\left(\lambda\sqrt{\pi}\,\mathrm{erf}\left(\frac{\lambda}{\upsilon}\right)+\upsilon e^{-\lambda^2/\upsilon^2}\right)\right], \quad (16)$$

where $\mathrm{erf}(x)=2\pi^{-1/2}\int_0^x e^{-t^2}dt$.

An example of $\lambda_{\mathrm{app}}(\lambda)$ dependence is shown in Fig. 1 for $\omega=5$ corresponding to our experimental geometry. As expected for $\lambda<1$, all of the segment can fit into the detection volume and $\lambda_{\mathrm{app}}\approx\lambda$). For $\lambda\gg 1$ the apparent length saturates at the value which can be found from (15),

$$\lambda_{\mathrm{app}}(\lambda\to\infty) = \omega\sqrt{\frac{\pi}{\omega^2-1}}\arctan\sqrt{\omega^2-1}. \quad (17)$$

At this point we would like to discuss the validity of the assumptions leading to Eq. (12). The main assumption we made was to neglect the internal dynamics within the labeled segment. This assumption, in fact, just puts a lower limit on the accessible range of studied segmental displacements: the derived equations are valid as long as the center-of-mass motion $\Delta\mathbf{r}(t)$ of the segment is larger than the characteristic motions *within* the segment.

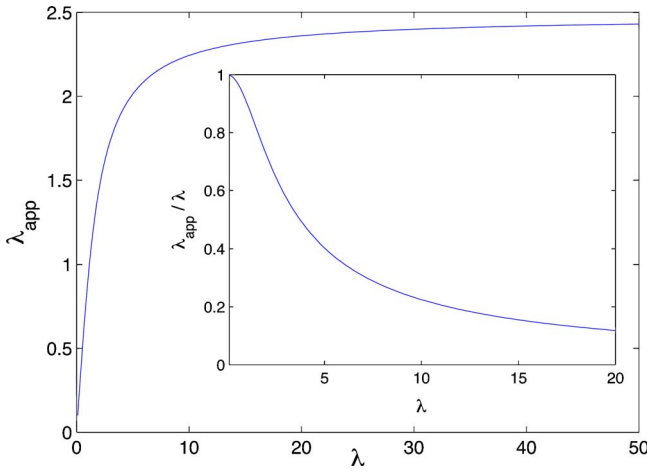

FIG. 1. (Color online) Dependence of the apparent length of the labeled segment on its real length as given by Eq. (16) for $\omega=5$ (close to the aspect ratio of the sampling volume in our setup). The lengths are given in the units of confocal volume radius $\lambda=L/w_{xy}$, $\lambda_{\mathrm{app}}=L_{\mathrm{app}}/w_{xy}$. The apparent length of very long $\lambda\gg 1$ segments approaches $\approx 2.5w_{xy}$. Inset: Ratio of the apparent length to the real length of the labeled segment. Labeled segment lengths of $L<w_{xy}(\lambda<1)$ result in $L_{\mathrm{app}}\approx L$.

The characteristic internal motions $\langle \Delta r_{\mathrm{int}}^2\rangle$ within the labeled segment can be estimated to be of the order of $\langle \Delta r_{\mathrm{int}}^2\rangle=(2/45)L^3/l_p$.[14] For segmental displacements larger than that, motions within the labeled part can be neglected and the labeled segment can be considered essentially rigid and moving as a single unit.

This condition seemingly prohibits studies with long labeled segments, which have considerable motions within them. However, only a small part of the filament (of length $\approx L_{\mathrm{app}}<L$) can cross the sampling volume and contribute to the fluctuations in fluorescence at any given moment. Thus the lower limit for the range of accessible segmental motions can be further relaxed to $(2/45)L_{\mathrm{app}}^3/l_p$. For example, even for very long homogeneously labeled actin filaments ($L\gg w_{xy}$, $L_{\mathrm{app}}\approx 2.5w_{xy}$) the segmental dynamics can be studied in the range $\langle \Delta r^2\rangle > 4\times 10^{-4}$ μm^2.

The expressions derived in this section [such as Eqs. (12), (13), and (15)] can be directly used to measure segmental displacements from FCS correlation functions: only the parameters defining the experimental geometry [w_{xy}, w_z, and in the case of Eq. (12) L in addition] need to be calibrated. All other parameters affect $G_2(t\to 0)$, the value of which can be determined from the plateau level of the experimentally measured correlation function at short time scales. Thus the correlation function depends essentially on the monomer displacements only $h_\perp^2$ and $h_\parallel^2$. Having two independent sets of FCS measurements, e.g., on partially labeled and homogeneously labeled filaments, one should be able in principle to determine each of the displacements $h_\perp^2$ and $h_\parallel^2$ separately as a function of time.

For our studies presented here, however, we will neglect the longitudinal displacement $h_\parallel^2$ in comparison with transverse motion $h_\perp^2$. Because of geometry of small deflections, the internal dynamics of stiff filaments with lengths l smaller

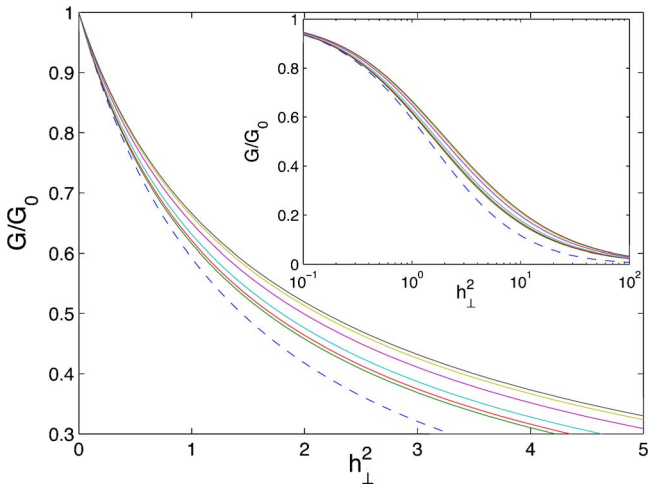

FIG. 2. (Color online) Calculated dependencies of FCS correlation function on the transverse mean-square displacement of semiflexible polymer segment. FCS correlation functions are normalized by their zero-time values (to have unit amplitude) and transverse MSD is given in the units of confocal volume radius $h_\perp^2=\langle\Delta r_\perp^2\rangle/w_{xy}^2$. The dashed curve is given by standard FCS expression Eq. (14) for isotropic motion. The other curves are calculated from Eq. (12) and its limiting cases, Eqs. (13) and (15), for different values of λ, left to right: 0, 1, 2, 5, 15, ∞. Inset: Same curves in semilog scale allowing to assess wider range of $h_\perp^2$.

than l_p is largely transverse. Based mostly on geometrical considerations Granek[14] evaluates $h_\parallel^2\approx 0.21(l/l_p)h_\perp^2$ [Eq. (C.16) in Granek's paper[14] and those related to it]. For filaments' length of $l\sim 6$ μm as in our experiments and F-actin persistence length $l_p\approx 17$ μm, we thus expect the longitudinal MSD to be an order of magnitude smaller than the transverse MSD. Furthermore, considerations of tension propagation within the filament[30] lead to even smaller longitudinal displacements over a wide range of internal dynamics. We note that at long time scales, where monomer displacements are dominated by the translational diffusion of the filament, $h_\parallel^2$ and $h_\perp^2$ should become comparable. However, most of the range of our measurements and, actually, most of our interest fall onto the range of internal filaments' dynamics, where the assumption of $h_\parallel^2\ll h_\perp^2$ is reasonably safe.

Then with known geometrical parameters and measured $G_2(t\to 0)$, Eq. (12) and its limiting cases, Eqs. (13) and (15), give a one-to-one relation between segmental MSD and FCS correlation function. Some examples of such dependence are given in Fig. 2. Using these dependencies, the experimentally measured correlation function $G_2(t)$ can be converted into the temporal dependence of segmental MSD $\langle\Delta r_\perp^2(t)\rangle$ $(=w_{xy}^2h_\perp^2(t))$.

Finally, we note that the failure to take into account the anisotropy of monomer motion in the calculation leads to the relations between $\langle\Delta r^2(t)\rangle$ and $G(t)$ which may deviate significantly from the correct ones. The problem is especially severe for pointlike labeling of the filaments: compare the dashed line in Fig. 2 for isotropic motion of pointlike sources to the leftmost solid line for anisotropic motion of pointlike labels. However, this problem is less severe for long labeled stretches. Indeed, the theory developed by Winkler *et al.*[20] for their recent FCS measurements assumes isotropic monomer motion, and thus their starting point is very different from ours. Nevertheless, for homogeneously labeled filaments and for a particular case of polymer dynamic theory, their expression for the correlation function [Eq. (50) in Winkler *et al.* paper[20]] is similar to our Eq. (15) for $L\to\infty$. The reasons for this agreement are quite clear: since the correlation function for long homogeneously labeled segments is essentially insensitive to longitudinal motion, the specific assumptions about the magnitude of longitudinal MSD (whether it is much smaller or is similar to transverse MSD) make little difference. Thus with respect to anisotropy of monomer motion, the analysis of data of Winkler *et al.* for homogeneously labeled filaments is quite proper. However, one should be cautious extrapolating their approach to partially labeled filaments.

III. MATERIALS AND METHODS

A. Actin preparation

Unlabeled actin is purified from chicken skeletal muscle acetone powder and stored in G-buffer.[31] Two sets of samples are prepared: (1) filaments labeled at defined positions and (2) homogeneously labeled filaments.

In order to label the filaments at defined positions (sample 1), we utilize fluorescently labeled actin filament seeds as templates for additional polymerization of unlabeled actin monomers. To prepare fluorescent seeds we first polymerize 1 μM of fluorescent G-actin (Actin Alexa 568, Molecular Probes, Eugene, OR, or rhodamine-actin, Cytoskeleton, Denver, CO) in the presence of phalloidin (Molecular Probes) to stabilize the filaments (1:1 actin to phalloidin molar ratio). The labeled filaments are then broken by a brief sonication and vigorous pipetting into short fragments (average length of ~170 nm, estimated by FCS, see Sec. IV). These fragments are then used as seeds for further polymerization of unlabeled G-actin (9 μM). Polymerization proceeds for 10 min at room temperature. We note that concurrent with polymerization, there is an ongoing annealing process[32] which both increases polymer length and creates multiply labeled filaments. Independent fluorescence microscopy observation[33] confirms that at the beginning of the experiment about 10% of filaments are labeled at two distinct positions (typically separated by more than 1 μm), while the rest are single labeled. Since the distance between the labeled portions of the double-labeled filaments is much larger than confocal radius (0.21 μm), the "cross-talk" between the labels can be neglected and the formalism derived in the preceding section can be applied.

The homogeneously labeled filaments (sample 2) are prepared in a similar manner. The difference is that the seeds are prepared from a mixture of labeled and unlabeled actin monomers (1:9 molar ratio) and further polymerization proceeds with the same mixture.

This procedure results in actin filaments of several microns in length: ~4 μm on average at the beginning of the experiment and growing in the course of experiment to ~8 μm due to annealing, as verified by fluorescence microscopy.[33]

For the experiments, the solution is diluted tenfold to a final actin concentration of 1 μM. Typically, 1 μl of solution

is sealed between two glass coverslips separated by a 250 μm spacer. To prevent protein adsorption, the glass coverslips are coated with an inert polymer (polyethylene glycol) according to the protocol of Perret *et al.*[34] Most of the measurements were carried out at a distance of 40 μm from the surface. This distance was chosen on purpose to be larger than F-actin length in order to minimize the effect of surface proximity on filament dynamics. Control experiments performed at a distance of 100 μm from the surface give results identical to those presented here.

The experiments are started immediately after dilution and are conducted within 30 min. The main reason to limit the duration of experiment is to minimize the effect of actin filament fragmentation, which leads to appearance of short filaments and associated noise in the FCS correlation function. After ~1 h of FCS measurement we start to see the changes in the MSD due to the fragmentation: the MSD versus time curve shifts to larger displacements. To be on the safe side, we limit all of our measurements to the first 30 min after polymerization.

At monomer concentration used in our experiments (1 μM) and for filament length in the 4–8 μm range, actin polymer solution is near the crossover from the dilute to semidilute regime.[35] Thus the actin filaments are expected to interact only weakly. Estimations[14,15] of the mesh size ($\xi \sim 1.4$ μm) and of the entanglement length (~2.3 μm) also point to only weak entanglement of the filaments at the scales of motion below 1 μm (so-called "loosely entangled" regime of semiflexible polymer solution[36]).

B. Experimental setup

The optical setup is home-built based on the Nikon Eclipse TE300 inverted microscope (Nikon Corporation, Tokyo, Japan). The confocal excitation is provided by 514 nm line (~2.5 μW power before microscope objective) of an Ar-ion laser (Advantage 163D, Spectra-Physics, Mountain View, CA) deflected by Q525 dicroic beam splitter (Chroma Technology, Rockingham, VT) into a high-power objective lens (UPLAPO 60X1.2W, Olympus Europe, Hamburg, Germany). The collected emission passes through the beam splitter, then a bandpass filter HQ565/80 (Chroma Technology, Rockingham, VT) and a pinhole of 25 μm in diameter. The emission is detected by a photon counting avalanche photodiode (SPCM- AQR-14 PerkinElmer Optoelectronics, Vaudreuil, Quebec, Canada) whose output is fed into digital correlator Flex2k-12Dx2 (Correlator.com, Bridgewater, NJ). The correlator is capable of working in two modes, either as traditional correlator carrying out the correlation analysis of emission online, or as photon history recorder, storing the time arrivals of every photon on computer hard drive. For the presented experiments, we make use of the photon history recorder mode, while analyzing the recorded photon traces offline with software correlator as described in Sec. III. The correlator program was written as C-MODULE running under MATLAB environment (MathWorks, Natick, MA).

The parameters $w_{xy} \approx 0.21$ μm, $w_z \approx 1.1$ μm of the confocal volume are calibrated before and after each experiment by measuring the diffusion of free Rh6G fluorophores.[28]

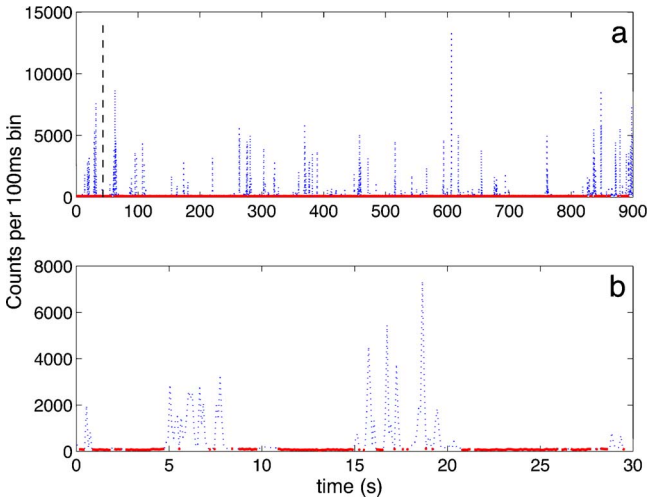

FIG. 3. (Color online) Photon count trace of partially labeled actin filaments (sample 1). The photon trace is collected with 16.7 ns resolution and split into 100 ms bins. The data points represent photon counts per bin. (a) Full trace over the duration of one measurement, (b) zoom into first 30 s of measurement. Bursts (dotted line) due to the passage of labeled parts are separated by the intervals of background noise (solid line).

C. Data analysis

Sample 1. The measurement of the photon emission count rate from locally labeled F-actin reveals that photons arrive in intense bursts of $\sim 10^5$ counts/s lasting ~0.1–1 s separated by intervals of low count rate of $\sim 10^3$ counts/s (Fig. 3). The bursts are caused by the passage of the labeled F-actin through the confocal volume. The fluorescence in between the bursts originates from residual free fluorophores diffusing in the sample. The motion of the free fluorophores results in a correlated background noise $I_b(t)$ which adds up with the labeled actin signal $I(t)$ to a total emission $I_{\mathrm{tot}} = I + I_b$. Thus the overall correlation function $G_{\mathrm{tot}}(t) = \langle \delta I_{\mathrm{tot}}(0)\, \delta I_{\mathrm{tot}}(t) \rangle$ is given by

$$G_{\mathrm{tot}}(t) = G(t) + G_b(t), \tag{18}$$

where $G(t) = \langle \delta I(0)\, \delta I(t) \rangle$ and $G_b(t) = \langle \delta I_b(0)\, \delta I_b(t) \rangle$ are the correlation functions of emission from labeled segments and from free fluorophores, respectively.

Although the overall contribution of free fluorophores G_b to the total correlation function is small, their fast motion is responsible for most of the decay of the correlation function at the time scales below 1 ms, where the motion of the filament segments is negligible. This could limit the analysis of monomers' MSD to the time scales above 1 ms. However, as shown below, it is possible to separate the contributions of labeled actin and free fluorophores within the *same* experiment, and thus, extend the range of measurements to time scales as low as ~40 μs.

In order to separate free fluorophore noise from the signal, we record the complete photon trace, i.e., times between arrivals of consecutive photons (with temporal resolution of 16.7 ns). The photons are then binned into 100 ms intervals $\{I(t_n)\}$ (Fig. 3). The stretches of time with no bursts are determined and the background correlation function $G_b(t)$ is calculated on these stretches using the original photon traces. The total correlation function $G_{\mathrm{tot}}(t)$ is computed using the

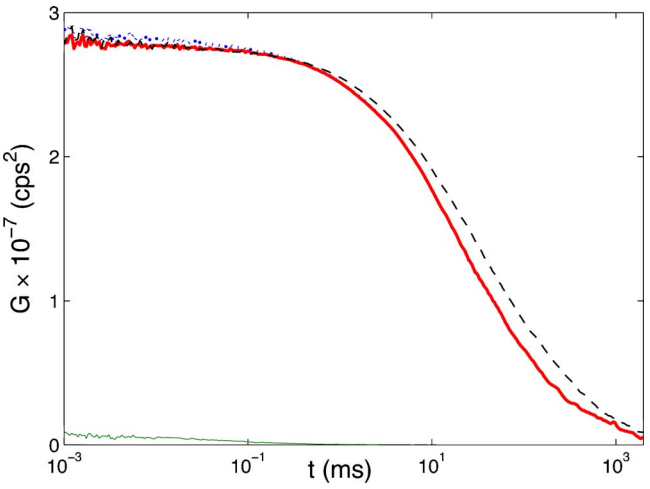

FIG. 4. (Color online) Total $G_{tot}(t)$ (dotted line), background $G_b(t)$ (thin solid line), and signal $G(t)$ (thick solid line) correlation functions of partially labeled filaments (sample 1). $G_{tot}(t)$ is obtained by analyzing the complete photon trace, $G_b(t)$ is caused by the diffusion of free fluorophore and is calculated from the photon trace in between the bursts in Fig. 3. $G(t)=G_{tot}(t)-G_b(t)$ is the correlation function resulting from the motion of F-actin labeled segments after background subtraction. The dashed line is the correlation function of homogeneously labeled actin (sample 2) after subtraction of background noise. The correlation function of sample 2 was normalized to have the same amplitude as that of sample 1 in order to facilitate the comparison of temporal behavior.

complete photon trace. Finally, the contribution of labeled actin $G(t)$ is obtained using Eq. (18). The intensity-normalized correlation function of actin segments is found by $G_2(t)=G(t)/(I_{tot}-I_b)$.

We find this procedure more robust than the correlation analysis of bursts intervals. First, there is some background contribution within the bursts as well. Second, unlike bursts, the intervals of pure background can be determined unambiguously: any intervals suspect to contain a burst can be deselected.

Practically, the background is deduced by calculating the median intensity over all bins $I_{med}=\text{median}(\{I(t_n)\})$ and selecting all of the intervals which deviate from the median by less than $\sigma=\text{median}(\{(I(t_n)-I_{med})^2\})$ for analysis of background noise. An example of this procedure is presented in Fig. 3. The resulting total, background, and signal correlation functions $G_{tot}(t)$, $G_b(t)$, and $G(t)$ are shown in Fig. 4. The background correlation function $G_b(t)$ is indeed well described by 3D diffusion model of the free fluorophore[28] with a characteristic decay time of 70 μs. We note that the amplitude of $G(t)$ is much larger than that of $G_b(t)$ mainly due to the multiple labeling of the filament segments: thus the motion of the labeled segments leads to much larger fluctuations in emission than the motion of single fluorophore molecules.

For calculation of monomers' MSD the amplitude of the correlation function $G_0=G(t\to 0)$ is estimated from the level of the correlation function in 3–20 μs range, which is above the characteristic time scales of the fluorophore triplet state kinetics and below the characteristic time scales of segmental dynamics.

Sample 2. We use the same approach to analyze data from homogeneously labeled F-actin. However, since the passage of the labeled segments through the sampling volume is more frequent in this case as compared to sample 1, we make use of shorter binning intervals of 30 ms and we pick the intervals with the average count rate not exceeding $I_{med}+0.25\sigma$ for the analysis of background noise. These conditions give a noise correlation function with characteristic decay time below 100 μs. The above parameters were found to be optimal between less restrictive conditions, which lead to a notable contribution of the signal in the estimated noise correlation function (characterized by decay times exceeding 1 ms), and more restrictive parameters, which clearly underestimate the noise level.

IV. RESULTS AND DISCUSSION

FCS correlation functions. We present the correlation functions obtained from both types of samples in Fig. 4. To facilitate the comparison of temporal kinetics, the amplitude of the correlation function of homogeneously labeled actin was adjusted to the level of the correlation function of the partially labeled sample. The functions look similar but are notably shifted in time: the correlation function of the homogeneously labeled sample decays slower by a factor of $\sim$1.4 than that of the locally labeled F-actin.

Estimation of apparent lengths. We can estimate the length of the labeled parts of sample 1 by analyzing the amplitude of its intensity-normalized correlation function $G_2(t\to 0)$. G_2 amplitude is 62 ± 8 times higher than the corresponding amplitude of the correlation function of G-actin monomers obtained in similar conditions (data not shown). Since 14 actin monomers form a filament of 37 nm, this gives the apparent length of the labeled segment of $L_{app}\approx 160\pm 20$ nm. Converting L_{app} into real segment length [Eq. (16) and Fig. 1] we obtain $L\approx 170\pm 30$ nm.

The apparent length of *homogeneously* labeled F-actin is $\sim$470 nm$\approx 2.3w_{xy}$, as estimated from the amplitudes of the corresponding correlation functions. This value is in a good agreement with our expectations for long homogenously labeled filaments [Eq. (16) and Fig. 1].

Monomer MSD. Since the correlation function for homogeneously labeled filaments is essentially insensitive to longitudinal displacement, the transverse monomer MSD can be directly determined from $G_2(t)$ in the case of sample 2. For partially labeled sample (sample 1), as discussed above, in order to extract the $\langle \Delta r_\perp^2(t)\rangle$ dependence from the correlation functions we neglect the longitudinal motion of the segments.

Although the general expression Eq. (12) can be used to analyze both sets of data, the numerical calculation shows that for $L<w_{xy}$ (i.e., $\lambda<1$) Eq. (12) leads to essentially the same dependence of the correlation function G_2 on MSD as Eq. (13) derived for $L\to 0$ (Fig. 2). Since in the case of partially labeled filaments the length of the labeled part ($\sim$170 nm) is smaller than $w_{xy}\approx 210$ nm, Eq. (13) can be used to calculate monomer MSD. Similarly, for homogeneously labeled filaments with length larger than 3 μm ($\lambda=L/w_{xy}>15$), Eq. (15) for infinitely long labeled segment can be used (compare curves for $\lambda>15$ and $\lambda\to\infty$ in Fig. 2). Thus we make use of the explicit expressions Eqs. (13) and (15), to analyze the data on partially and homogeneously

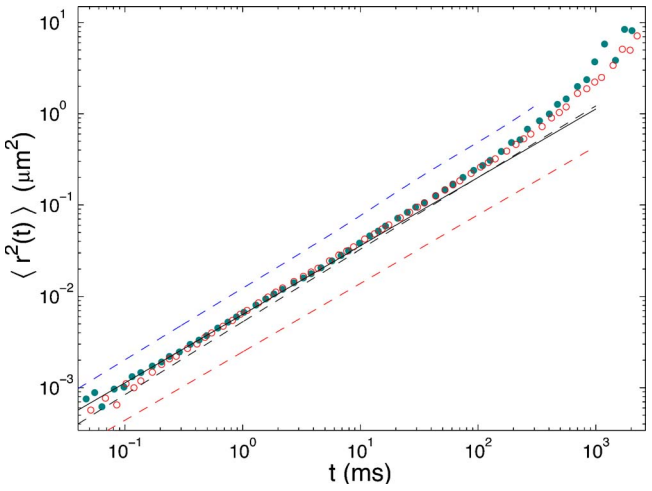

FIG. 5. (Color online) The kinetics of random motion $\langle \Delta r_\perp^2(t) \rangle$ of actin filaments' segments. Experimental measurements on locally labeled (full circles) and on homogeneously labeled (open circles) are compared to the theoretical predictions. Solid line: hydrodynamic theory of Kroy and Frey (Ref. 15). Dashed lines (top to bottom): hydrodynamic theories of Harnau *et al.* (Ref. 12), of Granek (Ref. 14) and nonhydrodynamic theory. The parameters used for the calculation are $l_p=17$ μm, filament diameter of 7 nm, solvent viscosity 1 mPa s, and filament length of 6 μm.

labeled polymers, respectively. For clarity, we rewrite these expressions in the form they are used for data analysis

$$\frac{G_2(h_\perp^2)}{G_2(t\to 0)} = \frac{\omega}{\sqrt{(1+h_\perp^2)(\omega^2-1)h_\perp^2}} \times \ln \frac{\sqrt{(1+h_\perp^2)\omega^2}+\sqrt{(\omega^2-1)h_\perp^2}}{\sqrt{\omega^2+h_\perp^2}} \tag{19}$$

for partially labeled samples, and

$$\frac{G_2(h_\perp^2)}{G_2(t\to 0)} = \frac{1}{\sqrt{1+h_\perp^2}\arctan\sqrt{\omega^2-1}} \arctan\sqrt{\frac{\omega^2-1}{1+h_\perp^2}} \tag{20}$$

for homogeneously labeled samples.

Practically, in both cases we set $\omega=w_z/w_{xy}$ to the value determined in the setup calibration (see Sec. III) and tabulate $G_2(h_\perp^2)/G_2(t\to 0)$ for a wide range of $h_\perp^2$ as exemplified in Fig. 2 (curves for $\lambda=0$ and $\lambda\to\infty$). We normalize the experimentally obtained correlation functions $G_2(t)$ by their plateau values. We use tabulated $G_2(h_\perp^2)/G_2(0)$ dependencies to find $h_\perp^2$ values corresponding to each measured data point $G_2(t)$. This gives the $h_\perp^2(t)$ dependence [and, respectively, $\langle \Delta r_\perp^2(t) \rangle = w_{xy}^2 h_\perp^2(t)$].

The extracted temporal dependencies of transverse monomer motion are presented in Fig. 5. The data span a wide range of time scales: from $\sim$40 μs to $\sim$2 s. Despite the difference in the temporal behavior of the original correlation functions for partially and homogeneously labeled filaments, the application of the appropriate expressions for each case leads to consistent data on monomers dynamics for both sets of measurements. The data for the two samples essentially coincide up to $\sim$0.3 s. At $t\gtrsim 0.3$ s, the data for partially labeled sample exhibit somewhat larger displacements than those for homogeneously labeled sample, probably indicating the effect of longitudinal diffusion in this range of time scales. We note that the longitudinal displacement is not equivalent to the difference in MSD in two data sets. In principle, it could be calculated from the measured correlation function of partially labeled sample using Eq. (12) together with $\langle \Delta r_\perp^2(t) \rangle$ obtained on homogeneously labeled sample. We are reluctant, however, to perform the calculation of $\langle \Delta r_\parallel^2 \rangle$ at this stage: the difference between $\langle \Delta r_\perp^2(t) \rangle$ calculated from two sets of data is not so large and, in addition, the (unknown) dispersion in the lengths of the labeled parts of sample 1 may significantly influence the result of such calculation (the effect of this dispersion on the calculation of transverse displacement is much smaller). Finally, we are not sure whether in this range the problem of separation of $\langle \Delta r_\perp^2 \rangle$ and $\langle \Delta r_\parallel^2 \rangle$ is well defined. (See discussion of *Fitting data in the whole range* further on.)

The monomers' MSD temporal dependence is close to $\langle \Delta r_\perp^2 \rangle \propto t^{0.79\pm0.01}$ kinetic law for time scales below $\sim$0.2 s and deviates from this dependence at longer times apparently due to the onset of the regime of translational diffusion of the filaments. Indeed, at the long time scales MSD kinetics is close to $\langle \Delta r_\perp^2 \rangle \propto t$.

Comparison to theories. Several theories predict monomer kinetics to follow $\langle \Delta r_\perp^2 \rangle \propto t^{0.75}$ law or very similar dependence.[10–15,37] There are differences in the predicted prefactors depending on the way the hydrodynamic interactions and boundary conditions are taken into account. In Fig. 5 we compare our results to several of the theories which give explicit expressions or detailed prescriptions on calculating $\langle \Delta r^2(t) \rangle$ dependence.

Simple treatments of the dynamics[13] taking into account the filaments' elasticity and local friction of polymer segments in solution and neglecting hydrodynamic interactions between segments leads to

$$\langle \Delta r^2 \rangle \approx 0.31 \left(\frac{k_B T}{\eta l_p^{1/3}} t \right)^{3/4}, \tag{21}$$

where η is solvent viscosity. While the numeric prefactor in Eq. (21) may slightly vary for different nonhydrodynamic theories, in general, nonhydrodynamics theories underestimate the segmental kinetics by a large factor [e.g., lower dashed line in Fig. 5 is given by Eq. (21) with $\eta=1$ mPa s, $l_p=17$ μm, and $T=293$ K].

Interestingly, even a simplified account for the hydrodynamic interactions within the filament leads to a good agreement between theory and the experimental results. Kroy and Frey[15,37] arrive at an expression similar to Eq. (21). However, they take into account hydrodynamic interactions by rescaling segmental friction coefficient by $\ln(\xi_h/a)$, where ξ_h roughly corresponds to the polymer mesh size ξ while a is filaments' diameter ($a\approx 7$ nm for bare F-actin)

$$\langle \Delta r_\perp^2 \rangle \approx 0.23 \left(\frac{k_B T \ln(\xi_h/a)}{\eta l_p^{1/3}} t \right)^{3/4}. \tag{22}$$

The curve (solid line) predicted by the above equation with $\xi=1.4$ μm corresponding to our experimental situation passes right through the experimental data points at the time

scales below ~10 ms and deviates from them slightly at longer time scales.

Granek[14] takes explicitly into account the hydrodynamic interactions between the distant segments and predicts a $\log(t)$ correction to the power law,

$$\langle \Delta r_{\perp}^2 \rangle \approx 0.082 \left(\ln \left[\frac{k_B T l_p \ln(l/\pi a)}{4\pi\eta a^4} t \right] \frac{k_B T}{\eta l_p^{1/3}} t \right)^{3/4}, \qquad (23)$$

where l is the polymer contour length. The middle dashed line in Fig. 5 is given by Eq. (23) with typical filaments' length $l=6$ μm [while it might be more appropriate to substitute the value of ξ instead of l in this case, in view of the double logarithmic dependence of $\langle \Delta r_{\perp}^2(t) \rangle$ on l, the precise value of l is of minor importance]. The theoretical predictions seem to grasp correctly the slope of the experimentally obtained curve and are offset by a small and almost constant factor (~20%) in the whole range below 100 ms.

Harnau *et al.* incorporate hydrodynamic interactions in another variant of their theory.[12] While Harnau *et al.* do not derive an explicit expression for $\langle \Delta r^2(t) \rangle$, they give detailed instructions on calculating monomers' MSD by summing up temporal correlation functions of normal modes of a fluctuating filament. The expressions for normal modes and their relaxation times are presented.[12] The normal mode relaxation times depend on the strength of hydrodynamic interactions which are evaluated by integrating preaveraged Rotne-Prager tensor[38] for hydrodynamic interactions for each normal mode over the length of a polymer. The upper dashed line in Fig. 5 is the result of our calculation of Harnau *et al.*[12] model for the MSD of a monomer in the interior of the filament. As above, parameters $\eta=1$ mPa s, $l_p=17$ μm, $T=293$ K, $l=6$ μm, and $a=7$ nm were used for solvent viscosity, filament persistence length, temperature, filament length, and filament diameter, respectively.[39] The calculated curve has a temporal dependence similar to that of the data and to the curve obtained from Granek theory.[14] However, quantitative agreement between the experimental data and the theory of Harnau *et al.*[12] is poor, with theory overestimating monomers'MSD by a factor of ~2 (see comment in Ref. 40). The disagreement between data and theory in this case can be traced to the fact that the theory of Harnau *et al.*[12] is aimed at describing the dynamics of long semiflexible polymers at the scales larger than polymer persistence length. Thus it can be expected to perform poorly in the case of motions below l_p as in the presented measurements. In particular, the theory of Harnau *et al.*[12] assumes a Gaussian chain at all the length scales, while the filaments at the scale $<l_p$ are rather linear. This leads to the overestimation of hydrodynamic interactions in the preaveraging approximation and as a result to the overestimation of monomers MSD.

Interestingly, the analysis of FCS data of Winkler *et al.*[20] on actin filaments is based on the theory of Harnau *et al.*,[12] and they use the characteristic time scale as one of the free parameters in their fitting procedures. A likely reason for the need to adjust the characteristic time scale is the overestimation of the hydrodynamic interactions discussed above.

Fitting data in the whole range. We mentioned already that the experimental MSD curves exhibit two regimes, that of internal dynamics with $\langle \Delta r_{\perp}^2 \rangle \propto t^{0.79}$ and translational diffusion with $\langle \Delta r_{\perp}^2 \rangle \propto t$. Thus it is tempting to fit the experimental data in the whole accessible range with the expressions which include both the filaments' internal dynamics and the translational diffusion. We do this with one important reservation: at long time scales, where translational diffusion takes over internal modes, the rotational diffusion of the whole filament may not be negligible either. We expect then that for monomer MSD $\gtrsim 1$ μm^2 some of the assumptions of our calculations may be valid only marginally, e.g., even the very concept of separation of transverse and longitudinal displacements may be ill defined at this scale of motion. Nevertheless, the fitting procedure in the whole range of data is not completely meaningless either: since the assumptions of the calculation just start to break down in the final decade of the probed time scales we would expect the fitted values of the diffusion coefficients to be at least reasonable (say correct within a factor of ~2–3).

The diffusion regime starts where the internal modes saturate. Thus one cannot use the integral approximations of type, Eqs. (22) and (23), to describe the internal dynamics in the whole range. Instead, the kinetics of all of the internal modes have to be summed up properly taking into account their eventual saturation. We did such fits for the three hydrodynamic theories already discussed in this section.

For Granek[14] and Kroy and Frey[15] theories the complete expressions for monomer MSD can be written in the following form:

$$\langle \Delta r_{\perp}^2 \rangle = \frac{4l^3}{\pi^4 l_p} \sum_{n=1}^{\infty} \frac{1}{n^4} (1 - \exp(-t/\tau_n)) + 4D_{\perp} t, \qquad (24)$$

where $D_{\perp}$ is the diffusion coefficient of the polymer in transverse direction and τ_n is the set of relaxation times of the normal modes (harmonic functions in both of the models). Our understanding is that the rotational diffusion would present itself in our measurements as an additional term in the transverse displacement of a segment. Thus it is possible that $D_{\perp}$, in fact, as calculated from our data carries both the kinetics of transverse and of rotational diffusions. In Granek theory the relaxation times depend on polymer length l and persistence length l_p,

$$\tau_n = \frac{4\eta l^4}{\pi^3 k_B T l_p n^4 \ln(L/\pi n a)}, \qquad (25)$$

whereas the expression for τ_n in Kroy and Frey theory[15] involves, in addition, the characteristic length ξ_h of hydrodynamic screening by the mesh,

$$\tau_n = \frac{4\eta l^4}{\pi^3 k_B T l_p n^4 \ln(\xi_h/a)}. \qquad (26)$$

In the case of Granek theory a good fit to the data with Eqs. (24) and (25) is achieved by using only two free parameters: the polymer length l and the diffusion coefficient $D_{\perp}$. All other parameters are set to the same values before ($\eta=1$ mPa s, $l_p=17$ μm, $T=293$ K, and $a=7$ nm). The solid line in Fig. 6 is a fit to the data on homogeneously labeled filaments with fit parameters $l=2.25\pm0.03$ μm and $D_{\perp}=0.52\pm0.01$ μm^2 s^{-1} (here and further the values of the fit

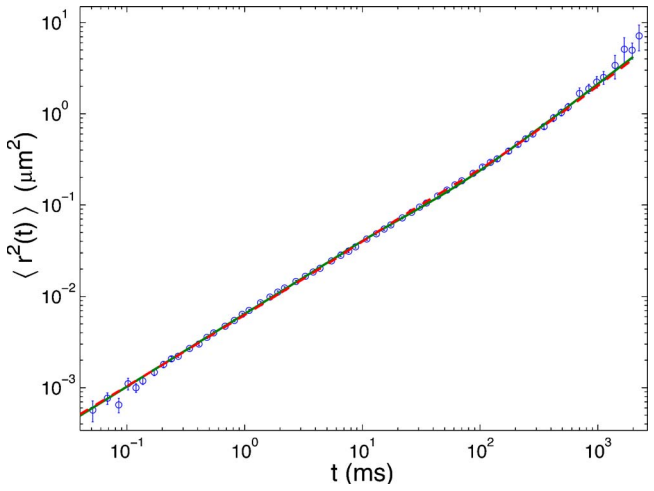

FIG. 6. (Color online) Theoretical fits to the experimental measurements of monomers' MSD Circles: data on homogeneously labeled actin filaments. Solid line: fit with Granek theory (Ref. 14). Fit line with the theory of Harnau *et al.* (Ref. 12) is almost indistinguishable from the solid line and is not drawn. Dashed line: fit with the theory of Kroy and Frey (Ref. 15). See text for the fitting parameters and discussion.

parameters to sample 2 data are given; the fits to sample 1 data give similar quality of fits and similar parameters). The fit is good overall, deviating slightly downwards from the data in the range around 100 ms. Thus fit somewhat shifts a crossover from internal dynamics to diffusion kinetics towards smaller time scales, which results in some underestimation of the filaments' length l. While the quality of the fit can be improved by invoking additional fitting parameters, we do not find this approach warranted by our data. The value of D allows to make an independent assessment of the filaments' length. In the framework of Granek theory the relation between $D_\perp$ and l is $D_\perp = k_B T \ln(l/a)/(4\pi\eta l)$. For $D_\perp = 0.52\ \mu\text{m}^2\,\text{s}^{-1}$ this gives $l \approx 3.9\ \mu$m, the value which is lower but roughly consistent with our fluorescence microscopy observations. The fact that fit to monomers' MSD underestimates l is probably a consequence of a wide distribution of filaments' length: the crossover range between internal and diffusion dynamics as well as the kinetics in the translational diffusion regime as measured by FCS are likely to be biased more by the smaller filaments in the distribution.

Equations (24) and (26) of Kroy and Frey theory carry three possible fitting parameters l, ξ_h, and $D_\perp$. In order to reduce the number of fitting parameters we use the expression for $D_\perp$ consistent with their theory: $D_\perp = k_B T \ln(\xi_h/a)/(4\pi\eta l)$, leaving us with two free fitting parameters: l and ξ_h. With the parameter values of $l = 2.70 \pm 0.05\ \mu$m and $\xi_h = 0.43 \pm 0.02\ \mu$m the quality of the fit (dashed line in Fig. 6) is very close to that of the fit with Granek theory: Kroy and Frey theory fits the data somewhat better in the range around 100 ms, while Granek theory performs slightly better around 1 s. Like in the case of Granek theory the estimated filaments' length is somewhat smaller than that measured by fluorescence microscopy. The value of ξ_h obtained from the fit is about thrice smaller than the estimated mesh size $\xi \sim 1.4\ \mu$m and is certainly reasonable.

The monomers' MSD in the theory of Harnau *et al.*[12] can be expressed in a way similar to Eq. (24). However, the mode amplitudes and their relaxation times are different, since the normal modes themselves are different from those used by Kroy and Frey[15] and Granek.[14] We were able to obtain a good fit to the experimental data with the theory of Harnau *et al.* using three fitting parameters: filaments' length, persistence length, and the diffusion coefficient. The fitting line is virtually indistinguishable from that of Granek theory and thus is not drawn in Fig. 6. While the fit values of filaments' length ($8.6 \pm 0.1\ \mu$m) and of diffusion coefficient ($0.35 \pm 0.01\ \mu\text{m}^2\,\text{s}^{-1}$) are rather reasonable, the F-actin persistence length is overestimated by a large margin ($270 \pm 10\ \mu$m). This overestimation appears to be solely the result of the overestimation of hydrodynamic interactions which we discussed above: the dependence of monomers' MSD on the persistence length is rather weak $\langle \Delta r_\perp^2(t) \rangle \propto l_p^{-1/4}$ [e.g., Eq. (21)] and the overestimation of hydrodynamic interactions by a factor of 2 would require fit value of $l_p \approx 17 \times 2^4 \approx 270\ \mu$m to compensate for the mistake.

Thus we find that the use of the theory of Harnau *et al.*[12] is inappropriate to describe the dynamics of stiff polymer chains below persistence length. As already mentioned, this is not really surprising since the theory[12] was designed for $l > l_p$ case. Remarkably though, the theory of Harnau *et al.* also fails to describe our data on the end-labeled DNA polymers[18] for which $l \gg l_p$ condition is well satisfied. In the range of time scales $\lesssim 3$ ms the end-monomer dynamics in DNA is seemingly unaffected by the hydrodynamic interactions between DNA segments, the feature which is not reproduced by the theory of Harnau *et al.* An interesting question (for which we have no answer) is whether the overestimation of the hydrodynamic interactions by theory at the scale below l_p could manifest itself also at the larger length scales.

Both Granek[14] and Kroy and Frey[15] theories describe our data well with only two fitting parameters and with the reasonable values of these parameters. Thus we are unable to make a choice between the two theories at this time. In fact, there is no essential contradiction between these two theories, they are rather similar, e.g., in their choice of normal modes. While in Granek theory (more precisely, the part of the theory that we make use of) the monomer motion is essentially uninhibited by the mesh, Kroy and Frey theory considers the polymer dynamics to be essentially affected by hydrodynamic screening properties of the mesh. For the loosely entangled regime such as in our measurements, both possibilities look rather plausible to us. The situation could be helped by having a theory relating the hydrodynamics screening length ξ_h to the mesh size ξ. Knowing which of these lengths is larger than the other could help to decide in the favor of one of the two theories in our experimental situation. On the experimental side, the measurements of F-actin dynamics at different monomer concentrations will help to resolve the issue.

Finally, we would like to return the question of longitudinal displacement versus transverse displacement. The consistence of the monomer MSDs calculated from FCS measurements on samples 1 and 2 under assumption $\langle \Delta r_\parallel^2 \rangle = 0$ indicates the that longitudinal displacements are indeed small: $\langle \Delta r_\parallel^2 \rangle \ll \langle \Delta r_\perp^2(t) \rangle$ (at least in the time range $\lesssim 0.3$ s). As discussed, we roughly expected this result based on the

considerations of filaments' stiffness. Admittedly, the agreement between the two sets of MSD data appears to be somewhat "too perfect" not allowing for any significant longitudinal displacement. It is possible that there are some additional (apart from filaments' stiffness) constrains on the longitudinal displacement. However, not having any further evidence we would like to avoid speculating on this issue.

To conclude, we adapt FCS formalism for the studies of the internal dynamics of semiflexible polymers. The formalism is based on the statistical properties of the filaments (their stiffness) and does not involve any specific model of polymer dynamics. The expressions relating monomers' MSD to FCS correlation functions are thus derived in a model-independent way. We make use of a developed formalism to obtain noninvasive measurements on the kinetics of segmental motion in actin filaments. Two labeling strategies, local labeling and homogeneous labeling, lead to consistent results. The transverse segmental MSD $\langle \Delta r_{\perp}^2(t) \rangle$ is probed over a wide range of timescales, from ~ 40 μs to ~ 2 s. Almost over the whole range the data points follow closely the prediction of hydrodynamic theories.[14,15] Thus, noninvasive measurements of $\langle \Delta r^2(t) \rangle$ carried out with FCS allow us to test hydrodynamic theories directly over a wide temporal range.

ACKNOWLEDGMENTS

We are indebted to R. Granek, E. Frey, and K. Kroy for fruitful discussions and for valuable suggestions. We thank also D. Groswasser for careful reading of the manuscript. This work has been supported by the Israel Science Foundation Grant Nos. 229/01 and 663/04.

[1] F. Gittes, B. Mickey, J. Nettleton, and J. Howard, J. Cell Biol. **120**, 923 (1993).
[2] T. Piekenbrock and E. Sackmann, Biopolymers **32**, 1471 (1992).
[3] J. Kas, H. Strey, and E. Sackmann, Nature (London) **368**, 226 (1994).
[4] L. LeGoff, O. Hallatschek, E. Frey, and F. Amblard, Phys. Rev. Lett. **89**, 258101 (2002).
[5] T. Gisler and D. A. Weitz, Phys. Rev. Lett. **82**, 1606 (1999).
[6] F. G. Schmidt, B. Hinner, and E. Sackmann, Phys. Rev. E **61**, 5646 (2000).
[7] A. Caspi, M. Elbaum, R. Granek, A. Lachish, and D. Zbaida, Phys. Rev. Lett. **80**, 1106 (1998).
[8] J. Y. Xu, A. Palmer, and D. Wirtz, Macromolecules **31**, 6486 (1998).
[9] I. Y. Wong, M. L. Gardel, D. R. Reichman, E. R. Weeks, M. T. Valentine, A. R. Bausch, and D. A. Weitz, Phys. Rev. Lett. **92**, 178101 (2004).
[10] G. Allegra and F. Ganazzoli, J. Chem. Phys. **74**, 1310 (1981).
[11] E. Farge and A. C. Maggs, Macromolecules **26**, 5041 (1993).
[12] L. Harnau, R. G. Winkler, and P. Reineker, J. Chem. Phys. **104**, 6355 (1996).
[13] L. Harnau, R. G. Winkler, and P. Reineker, J. Chem. Phys. **106**, 2469 (1997).
[14] R. Granek, J. Phys. II **7**, 1761 (1997).
[15] K. Kroy and E. Frey, Phys. Rev. E **55**, 3092 (1997).
[16] D. C. Morse, Phys. Rev. E **58**, R1237 (1998).
[17] F. Gittes and F. C. MacKintosh, Phys. Rev. E **58**, R1241 (1998).
[18] R. Shusterman, S. Alon, T. Gavrinyov, and O. Krichevsky, Phys. Rev. Lett. **92**, 048303 (2004).
[19] D. Lumma, S. Keller, T. Vilgis, and J. O. Radler, Phys. Rev. Lett. **90**, 218301 (2003).
[20] R. G. Winkler, S. Keller, and J. O. Rädler, Phys. Rev. E **73**, 041919 (2006).
[21] D. Magde, E. Elson, and W. Webb, Phys. Rev. Lett. **29**, 705 (1972).
[22] E. L. Elson and D. Magde, Biopolymers **13**, 1 (1974).
[23] D. Magde, E. L. Elson, and W. W. Webb, Biopolymers **13**, 29 (1974).
[24] E. Haustein and P. Schwille, Methods **29**, 153 (2003).
[25] N. L. Thompson, A. M. Lieto, and N. W. Allen, Curr. Opin. Struct. Biol. **12**, 634 (2002).
[26] *Fluorescence Correlation Spectroscopy: Theory and Applications*, edited by R. Rigler and E. Elson (Springer, Berlin, 2001).
[27] O. Krichevsky and G. Bonnet, Rep. Prog. Phys. **65**, 251297 (2002).
[28] R. Rigler, U. Mets, J. Widengren, and P. Kask, Eur. Biophys. J. **22**, 169 (1993).
[29] B. J. Bern and R. Pecora, *Dynamic Light Scattering* (Wiley, New York, 1976).
[30] R. Everaers, F. Julicher, A. Ajdari, and A. C. Maggs, Phys. Rev. Lett. **82**, 3717 (1999).
[31] J. D. Pardee and J. A. Spudich, Methods Enzymol. **85**, 164 (1982).
[32] E. Andrianantoandro, L. Blanchoin, D. Sept, J. A. McCammon, and T. D. Pollard, J. Mol. Biol. **312**, 721 (2001).
[33] For fluorescence microscopy observations the whole filament has to be visualized. Thus the samples are polymerized from totally fluorescent seeds as in sample 1 procedure. However, the polymerization mixture had 1:9 fluorescent to nonfluorescent G-actin. This preparation results in overall labeled filaments with bright spots marking the places of former seeds. For microscopy visualization and length measurements the solutions were diluted to 0.1 μM actin concentration (ten times smaller than for FCS measurements).
[34] E. Perret, A. Leung, A. Morel, H. Feracci, and P. Nassoy, Langmuir **18**, 846 (2002).
[35] J. J. Magda, H. T. Davis, and M. Tirrell, J. Chem. Phys. **85**, 6674 (1986).
[36] D. C. Morse, Macromolecules **31**, 7030 (1998).
[37] E. Frey, K. Kroy, and J. Wilhelm, in *Advances in Structural Biology*, edited by S. K. Mathotra and J. A. Tuszynski (Jai, London, 1998), Vol. 5.
[38] J. Rotne and S. Prager, J. Chem. Phys. **50**, 4831 (1969).
[39] We note here that for the weakly entangled solutions such as our samples, it is might be more appropriate to use mesh size ξ as an upper cutoff when evaluating hydrodynamic interactions and to use polymer length l for the calculation of eigenmodes in the theory of Harnau *et al.* However, there is almost no difference in the net result for monomers' MSD when separating ξ and l length scales as compared to the calculation with a single parameter l as put forward in the original theory (Ref. 12).
[40] Since we believe that the longitudinal displacement is much smaller than the transverse one, we compare measured $\langle \Delta r_{\perp}^2(t) \rangle$ to the theoretical predictions of Harnau *et al.* (Ref. 12) for full displacement $\langle \Delta r^2(t) \rangle$. It might be more fair to compare the measured $\langle \Delta r_{\perp}^2(t) \rangle$ to the expectation for the transverse displacement, which in the framework of the theory of Harnau *et al.* would equal $(2/3)\langle \Delta r^2(t) \rangle$. While we are ambivalent on this issue, both types of comparison lead to essentially the same conclusions.